Journal of Hazardous Materials 186 (2011) 1615–1624

Contents lists available at ScienceDirect

Journal of Hazardous Materials

journal homepage: www.elsevier.com/locate/jhazmat

Adsorption performance of VOCs in ordered mesoporous silicas with different pore structures and surface chemistry

Baojuan Dou[a], Qin Hu[a], Jinjun Li[a], Shizhang Qiao[b], Zhengping Hao[a,*]

[a] Department of Environmental Nano-Materials, Research Center for Eco-Environmental Sciences, Chinese Academy of Sciences, Beijing 100085, PR China
[b] ARC Centre of Excellence for Functional Nano-Materials, Australian Institute for Bioengineering and Nanotechnology, The University of Queensland, Brisbane QLD 4072, Australia

ARTICLE INFO

Article history:
Received 17 September 2010
Accepted 10 December 2010
Available online 17 December 2010

Keywords:
Ordered mesoporous silicas
Functionalization
Pore structure
Hydrophobicity
VOCs adsorption

ABSTRACT

Ordered mesoporous silicas with different pore structures, including SBA-15, MCM-41, MCM-48 and KIT-6, were functionalized with phenyltriethoxysilane by a post-synthesis grafting approach. It was found that phenyl groups were covalently anchored onto the surface of mesoporous silicas, and the long-range ordering of the mesoporous channels was well retained after the surface functionalization. The static adsorption of benzene and the dynamic adsorption of single component (benzene) and bicomponent (benzene and cyclohexane) on the original and functionalized materials were investigated. As indicated by the adsorption study, the functionalized silicas exhibit improvement in the surface hydrophobicity and affinity for aromatic compounds as compared with the original silicas. Furthermore, the pore structure and the surface chemistry of materials can significantly influence adsorption performance. A larger pore diameter and cubic pore structure are favorable to surface functionalization and adsorption performance. In particular, the best adsorption performance observed with phenyl-grafted KIT-6 is probably related to the highest degree of surface functionalization, arising from the relatively large mesopores and bi-continuous cubic pore structure which allow great accessibility for the functional groups. In contrast, functionalized MCM-41 exhibits the lowest adsorption efficiency, probably owing to the small size of mesopores and 1D mesoporous channels.

1. Introduction

Volatile organic compounds (VOCs) have been extensively involved in many industrial processes, whereas such compounds are hazardous to human health, contributing to serious environmental problems such as the destruction of the ozone layer, photochemical smog and global warming [1,2]. Hence the emission of VOCs has triggered increasing awareness focused on the development of abatement technologies to comply with the latest environmental regulations. Among the different alternatives available to remove VOCs, adsorption technology with no chemical degradation has been generally recognized as a preferred strategy, especially in cases where the organic pollutants to be captured have alternative uses [3]. The primary requirements of an adsorbent adopted in the industry process include sufficient adsorptive capacity, high adsorption rate, and strong hydrophobicity [4]. Activated carbon is widely employed in adsorption process owing to its high micropore volume and low operating cost [5]. Unfortunately, activated carbon often suffers from added fire risk, pore blocking, hygroscopicity and a lack of regenerative ability [6].

As a result, alternative adsorbents such as hydrophobic zeolite and mesoporous silica have attracted considerable attention to control VOCs. Hydrophobic zeolites have been found to be effective in VOCs removal [7,8]. However, serious diffusion restrictions imposed by the micropores (<2 nm) tend to inhibit its ability to adsorb large VOC molecules [9]. Ordered mesoporous silicas offer excellent features such as large pore volume and high surface area, narrow pore size distribution, open pore structure and reliable desorption performance [10–12]. Siliceous SBA-15, MCM-41, MCM-48 and KIT-6 are considered as representatives of mesoporous materials. SBA-15 and MCM-41 possess a two-dimensional (2D) hexagonal array of uniform cylindrical mesopores (*p6m*), while MCM-48 and KIT-6 consist of three-dimensional (3D) bicontinuous cubic arrangement of mesopores (*Ia3d*). In particular, studies found that the porous structure of SBA-15 not only consists of ordered mesopores but also of much smaller complementary pores connecting adjacent mesopore channels [13,14]. Similarly, the two intertwined systems of mesoporous channels in KIT-6 can also be connected through irregular micropores in the walls [15]. Previous studies have indicated that the bimodal materials (SBA-15 and KIT-6) have high affinity for various VOCs due to their complementary micropores, which are favorable to the diffusion process [10,16].

* Corresponding author. Tel.: +86 10 62923564; fax: +86 10 62923564.
E-mail address: zpinghao@rcees.ac.cn (Z. Hao).

0304-3894/$ – see front matter © 2010 Elsevier B.V. All rights reserved.
doi:10.1016/j.jhazmat.2010.12.051

In fact, the silanols (Si–OH) on the amorphous walls surface make original mesoporous silicas less hydrophobic and decrease the adsorption capacity of VOCs in the presence of water vapor, which limit their applications in the field of adsorption. Furthermore, surface siloxanes of original silicas may hydrolyze to silanols by water adsorption [17,18]. Therefore, surface chemistry tailoring is required for mesoporous silicas in order to improve hydrophobicity and selectivity for VOCs. One important way of modifying the surface chemistry is organic functionalization [13]. It has been established that the introduction of organic groups in the framework of nanoporous material has a positive effect on VOCs removal [19].

Surface functionalization can be conducted in three various ways such as subsequent surface functionalization of pre-fabricated silica materials ("grafting"), the simultaneous condensation of corresponding silica and organosilica precursors groups ("co-condensation") and the incorporation of organic groups as bridging components into the pore walls ("production of periodic mesoporous organosilica") [20]. Compared with the other two pathways, the grafting method, carried out by reaction of organosilanes with surface silanol groups, can maintain the original mesoporous structure. Adjustment of the surface chemistry of porous silicas with organic groups, such as alkyl chains or phenyl groups, can enhance the surface hydrophobicity [13]. Much progress focusing on the post-synthetic functionalization of mesoporous materials with organic groups and the corresponding applications has been made [17,21–24]. Zhao and Lu [21] demonstrated that surface functionalization of siliceous MCM-41 by grafting with trimethylchlorosilane (TMCS) was an effective technique in tailoring adsorbents for the selective abatement of VOCs from wastewater. However, there is very limited information available in the literature relating to the application of such inorganic-organic mesoporous solids in the field of VOCs removal, especially in gas steams. Furthermore, the effect of pore structure on the surface functionalization is essential for the synthesis of functionalized silicas and the corresponding VOCs adsorption.

The objective of this work is to investigate the surface functionalization and adsorption performances of ordered mesoporous silicas with different pore structures, including SBA-15, MCM-41, MCM-48 and KIT-6. The functionalized mesoporous silicas were synthesized by post-synthetic treatment with phenyltriethoxysilane (PTES). The dynamic and static adsorption behaviors of VOCs on the original pure silicas and functionalized silicas were investigated by continuous-flow adsorption measurements and digital microbalance, respectively. With regard to the dynamic adsorption, besides single component adsorption of benzene, competitive adsorptions of benzene with water or cyclohexane were also conducted to explore the affinity between VOCs molecules and functional groups on the mesoporous silica surface.

2. Experimental

2.1. Preparation of mesoporous silicas

Four mesoporous silicas, including SBA-15, MCM-41, MCM-48 and KIT-6 were synthesized according to the procedures described in the literature [25–28]. The nonionic Pluronic P123 ($EO_{20}PO_{70}EO_{20}$) was used as a template for the synthesis of SBA-15 and KIT-6, whereas the cetyltrimethyammonium bromide (CTAB) was used for MCM-41 and MCM-48. After being stirred, the solution mixture was transferred into a Teflon-lined autoclave and hydrothermally treated. The obtained solid products were collected by filtration, dried in air and then calcined at 550 °C for 6 h.

2.2. Surface functionalization with PTES

In a typical functionalization procedure, mesoporous silicas including SBA-15, MCM-41, MCM-48 and KIT-6 were degassed at 150 °C for 24 h under a vacuum condition. 1 g of dried silica sample was added to 50 mL of toluene and 5 mL of PTES followed by refluxing at 110 °C for 24 h. The obtained functionalized silicas were filtered, thoroughly washed with ethanol and dried in vacuum at 100 °C. The functionalized samples with PTES were designated as p-SBA-15, p-MCM-41, p-MCM-48 and p-KIT-6, respectively.

2.3. Characterizations

The XRD patterns of original and functionalized mesoporous silicas were recorded on a Siemens D5005 diffractometer with Cu Ka radiation ($\lambda = 0.1541$ nm) at 40 kV and 40 mA. Adsorption and desorption isotherms of nitrogen were measured with a NOVA 1200 gas sorption analyzer at liquid nitrogen temperature (−196 °C). Before measurements, all of the samples were degassed under vacuum condition at 120 °C for 18 h. The Brunauer–Emmett–Teller (BET) method was utilized to calculate the specific surface area using adsorption data acquired at a relative pressure (P/P_o) range of 0.05–0.25. The total pore volume was estimated from the amount adsorbed at a relative pressure of about 0.99. The pore size distribution curves were calculated from the analysis of the desorption branch of the isotherm based on the Barrett–Joyner–Halenda (BJH) algorithm. The micropore volume and micropore surface area were estimated by a t-plot method. Fourier transform infrared (FT-IR) spectra were measured by the KBr method recorded on a Bruker Tensor 27, scanned from 4000 to 600 cm^{-1}. The thermogravimetry (TG) and derivative thermogravity (DTG) analyses of original and functionalized silicas were performed on TG/DTA analyser (Setaram, Labsys). The heating rate was 10 °C min^{-1} from 30 °C to 900 °C under an air flow of 30 mL min^{-1}. Transmission electron microscopy images were collected on a JEOL 2011 microscope at 200 kV.

2.4. Dynamic adsorption measurements

The dynamic adsorption was carried out by a flow method reported by Hu et al. [29]. About 100 mg of sample was crushed into granules (40 to 60 mesh) and then loaded in a fixed-bed reactor. Before adsorption measurements, samples were degassed at 120 °C overnight under vacuum condition to remove the physically adsorbed water molecules and small organic impurities. Nitrogen was taken as a carrier gas and adjusted to keep a total flow rate of 100 mL min^{-1}. Adsorption performances of 1000 ppm benzene were conducted under both dry and wet conditions. To observe the effect of water vapor on the adsorption behaviors of the original and functionalized mesoporous silicas, the test gas consisting of nitrogen and 1000 ppm of benzene under the relative humidity (RH) of 13% was passed through the adsorption bed. To estimate the affinity between benzene molecules and phenyl groups on the surface of functionalized silicas, dynamic adsorption of bi-component (500 ppm of benzene and 500 ppm of cyclohexane, respectively) for siliceous materials before and after functionalization was conducted. The adsorbed amount of adsorbate was determined by the concentration change before and after adsorption measurements, tested by using a gas chromatograph (GC) equipped with a flame ionization detector.

2.5. Static adsorption measurements

Static adsorption equilibrium measurements of benzene on the original and phenyl-grafted mesoporous silica samples were recorded on an Intelligent Gravimetric Analyzer (model IGA-002,

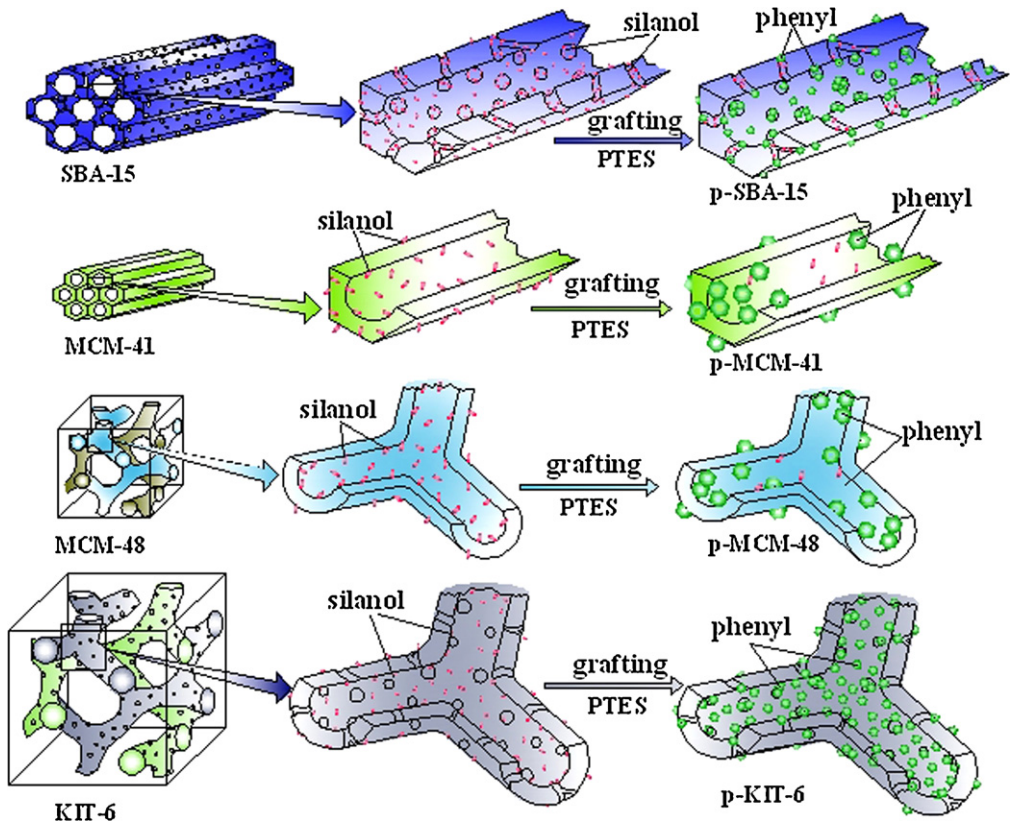

Fig. 1. Schematic representations of the surface functionalization for SBA-15, MCM-41, MCM-48 and KIT-6 with PTES.

Hiden Isochema Instrument) with a sensitivity of 0.1 μg. The apparatus has an ultrahigh vacuum system with a fully computerized microbalance allowing adsorption isotherms and the corresponding kinetics for each pressure increment to be determined, by the approach of monitoring equilibrium in real time using a computer algorithm [30]. Before adsorption measurements, the samples were degassed overnight at 120 °C in vacuum.

3. Results and discussion

3.1. Characterization of samples

During the post-grafting functionalization process, organic functional groups could be covalently attached to the silanol groups (Si–OH) on the external and inner pore surface in the presence of non-polar solvent, as schematically shown in Fig. 1. Powder low-angle XRD patterns of original and phenyl-grafted SBA-15, MCM-41, MCM-48 and KIT-6 are depicted in Fig. 2. Before grafting phenyl groups, SBA-15 and MCM-41 display three well-defined peaks, which can be indexed as (1 0 0), (1 1 0) and (2 0 0) diffractions, respectively, confirming a 2D hexagonal arrangement of mesopores (*p*6*m*) [31,32]. For MCM-48 and KIT-6, the XRD patterns represent three reflections, which can be assigned to the (2 1 1), (2 2 0) and (3 3 2) planes of a 3D cubic structure (*Ia*3*d*) [17,33]. After grafting phenyl groups onto the surface, peak positions of all the samples remain virtually constant, which is an evidence for maintaining the structural characteristics of the original silicas. As can be seen in Fig. 2, after functionalization, both MCM-41 and MCM-48 exhibit obvious decrease in the XRD peak intensities, while the decrease for MCM-41 is more significant than that for MCM-48, probably owing to the partial pore blockage in MCM-41 by the introduction of functional groups. However, the peak intensities of p-SBA-15 and p-KIT-6 show slight changes compared with those of their original materials, indicating that the surface functionalization with PTES has little effect on their mesostructures.

Shown in Fig. 3a and b are the nitrogen adsorption and desorption isotherms and the corresponding pore size distributions of

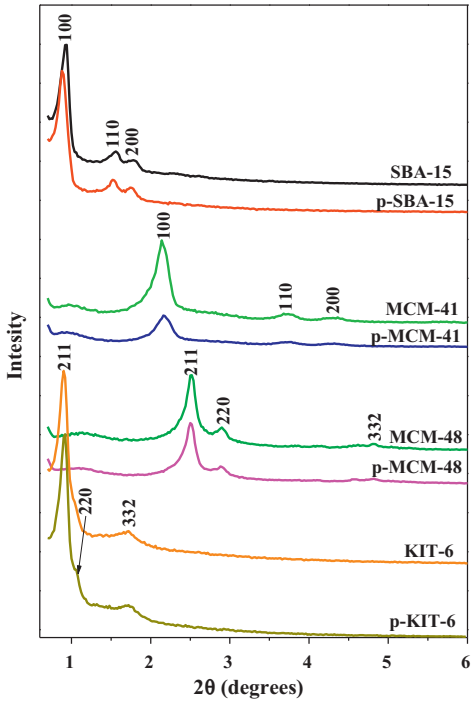

Fig. 2. XRD patterns of the original and phenyl-grafted SBA-15, MCM-41, MCM-48 and KIT-6.

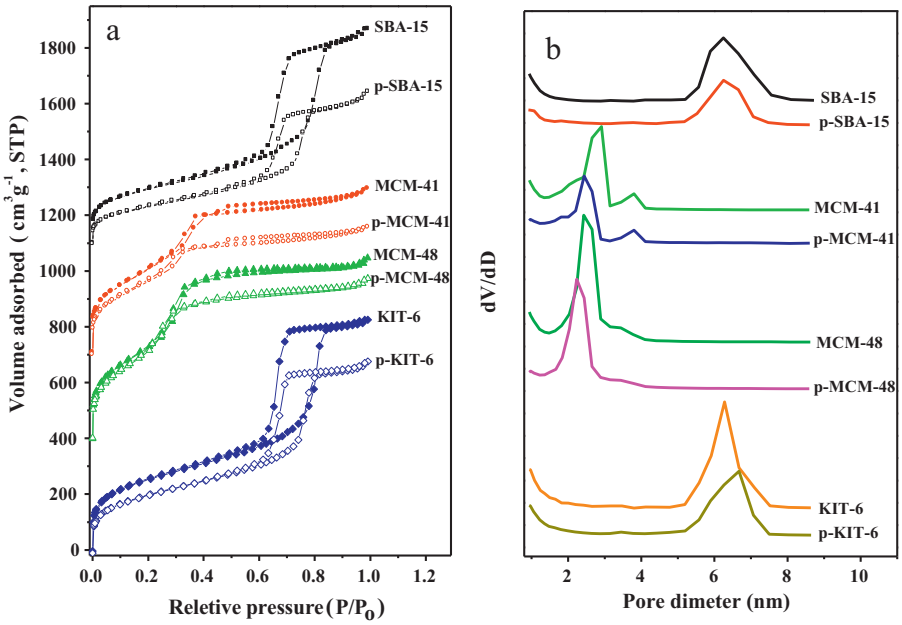

Fig. 3. Nitrogen adsorption/desorption isotherms (a) and BJH pore size distributions (b) for the original and phenyl-grafted SBA-15, MCM-41, MCM-48 and KIT-6. The isotherms for the original and phenyl-grafted MCM-48, MCM-41 and SBA-15 are shifted by 400, 700 and 1100 $cm^3\ g^{-1}$ STP, respectively.

original and phenyl-grafted SBA-15, MCM-41, MCM-48 and KIT-6, respectively. In Fig. 3a, it is apparent that all of the adsorption isotherms are of type IV (IUPAC classification), with a sharp capillary condensation step at intermediate P/P_o, indicating the presence of uniform mesopores [34]. Despite the decrease in the adsorbed amount of nitrogen, the shapes of the hysteresis loops for phenyl-grafted samples remain the same as those before functionalization, implying that the functionalization does not change the pore shapes of the silicas [35]. For SBA-15 and KIT-6 before and after functionalization, well-defined H1-type hysteresis loops are observed. This type of hysteresis loops is associated with capillary condensation and desorption in open cylindrical mesopores [36]. However, the capillary condensation and evaporation are nearly reversible for original and phenyl-grafted MCM-41 and MCM-48 owing to their relatively small mesopore size (<3 nm, Table 1). As can be seen in Table 1, the post-synthetic functionalization can reduce the surface area and the total pore volume to some extent, depending on the pore structure. With complementary micropores in the walls, the functionalization of hexagonal SBA-15 reduces its surface area and total pore volume by 27.4% and 28.1%, respectively, while the reductions for cubic KIT-6 are 17.7% and 17%, respectively, probably owing to the phenyl groups attached onto the mesopore surface and the blockage of micropores. Similarly, the functionalization reduces the surface area and the total pore volume of hexagonal MCM-41 by 12.7% and 22.5%, respectively, which are higher than those of cubic MCM-48 of 3.8% and 12.3%. This observation can be attributed to the effects of silica pore structures on the surface functionalization, as intuitively depicted in Fig. 1. The lesser degree of reduction for KIT-6 and MCM-48 can be ascribed to their two mutually interwoven and branched mesoporous channels, which provide more favorable mass transfer for functional PTES species through the mesopores and lead to less pore blockage compared with 2D mesostructure of SBA-15 and MCM-41. Even with larger mesopores than MCM-41 and MCM-48, SBA-15 and KIT-6 represent more remarkable decrease, suggesting that the complementary micropores in walls of SBA-15 and KIT-6 are more prone to blockage than the mesopores in MCM-41 and MCM-48.

The FT-IR spectra measurements prove the successful covalent grafting of the organic groups onto the silica wall [36]. Shown in Fig. 4 are the FT-IR spectra patterns of original and phenyl-grafted SBA-15, MCM-41, MCM-48 and KIT-6, respectively. In comparison to the original silicas, some new bands were detected in the functionalized materials. The bands at 3078 and 3058 cm^{-1} are attributed to the C–H stretching vibrations of the phenylene groups, while the bands at 1486, 1449, 1433 and 1395 cm^{-1} are attributed to the C=C vibration of the aromatic ring [37], and the bands at 740 and 700 cm^{-1} are assigned to the distinctive marks of benzene. It should be noted that the intensities of the adsorption peaks at about 3744 cm^{-1}, which is ascribed to free Si–OH groups [21], decrease significantly after functionalization, suggesting the occurrence of grafting reaction between Si–OH groups and organosilanes during the functionalization process.

The amount of organic functional groups incorporated into the mesoporous silicas was determined by thermogravimetric analy-

Table 1
Textural properties of the original and phenyl-grafted mesoporous materials.

Samples	BET surface area ($m^2\ g^{-1}$)	Pore diameter[a] (nm)	Total pore volume ($cm^3\ g^{-1}$)	Micropore volume ($cm^3\ g^{-1}$)	Micropore area ($m^2\ g^{-1}$)
SBA-15	698	6.3	1.20	0.07	146
p-SBA-15	506	6.3	0.86	0.02	43
MCM-41	1088	2.9	0.92	–	–
p-MCM-41	950	2.4	0.71	–	–
MCM-48	1210	2.4	1.02	–	–
p-MCM-48	1164	2.2	0.89	–	–
KIT-6	912	6.3	1.29	0.13	271
p-KIT-6	751	6.3	1.07	0.09	193

[a] Calculated using the Barrett–Joyner–Halenda (BJH) model based on the desorption branch of the isotherm.

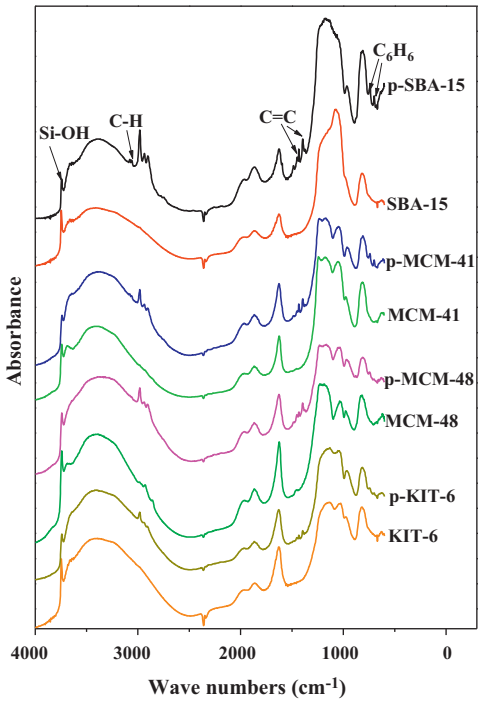

Fig. 4. FT-IR spectra of patterns of the original and phenyl-grafted SBA-15, MCM-41, MCM-48 and KIT-6.

sis, as shown in Fig. 5. The weight loss at temperature lower than 150 °C is attributed to the loss of adsorbed water [38]. In comparison with original samples, the phenyl-grafted silicas show an increased weight loss on TG curves and additional peaks on the corresponding DTG curves in the temperature region of 300–600 °C, due to the decomposition of the phenyl groups anchored onto the silica surface. It can be seen that the phenyl-grafted KIT-6 exhibits the highest weight loss between 300 and 600 °C, demonstrating the highest degree of surface functionalization.

Fig. 6 shows the TEM images of phenyl-grafted SBA-15, MCM-41, MCM-48 and KIT-6. Along the [1 0 0] direction the TEM images of p-SBA-15 (Fig. 6a) and P-MCM-41 (Fig. 6b) show that the ordered 2D hexagonal mesostructures (*P6m*) were preserved. Similarly, the cubic mesostructures (*Ia3d*) of p-MCM-48 and p-KIT-6 are confirmed by the TEM images of Fig. 6c and d, recorded along [1 0 0] and [1 1 1] respectively. The TEM results combined with nitrogen adsorption, XRD, FT-IR and TGA results confirm that the long-range ordered arrangement of the mesoporous channels are well retained after phenyl groups covalently anchored onto the silica surface.

3.2. Dynamic adsorption of single component

The removal of typical VOCs, such as benzene, by original and phenyl-grafted SBA-15, MCM-41, MCM-48 and KIT-6 was investigated by studying the adsorption breakthrough. The investigation was first undertaken for single component adsorbate with a low concentration under dry and wet conditions respectively to identify the performance of dynamic VOCs removal (Fig. 7). Generally, the longer the breakthrough time is, the higher the dynamic adsorption capacity becomes [10]. In the case of dry condition, all the phenyl-grafted mesoporous silicas exhibit shorter breakthrough time for benzene as compared with their original samples, which can be attributed to the decrease of surface areas and pore volumes caused by the surface functionalization. With respect to the experiments performed in humid environment (13% RH), the dynamic adsorption of benzene on the original and phenyl-grafted materials show different adsorption behaviors. In Fig. 7d, the breakthrough time for p-KIT-6 (~35 min) is longer than that for original KIT-6 (~30 min) in the presence of water vapor, in spite of comparatively lower surface area and pore volume of p-KIT-6. However, with the same bicontinuous cubic pore system but relatively small pore size compared with KIT-6, original and phenyl-grafted MCM-48 show similar breakthrough time (Fig. 7c). Shorter breakthrough times were observed for phenyl-grafted SBA-15 (Fig. 7a) and MCM-41 (Fig. 7b) as compared with their original samples, which is probably due to the significant reduction of pore volume by the functionalization. In addition, the post-breakthrough curves of the original and phenyl-grafted KIT-6 for benzene adsorption increase

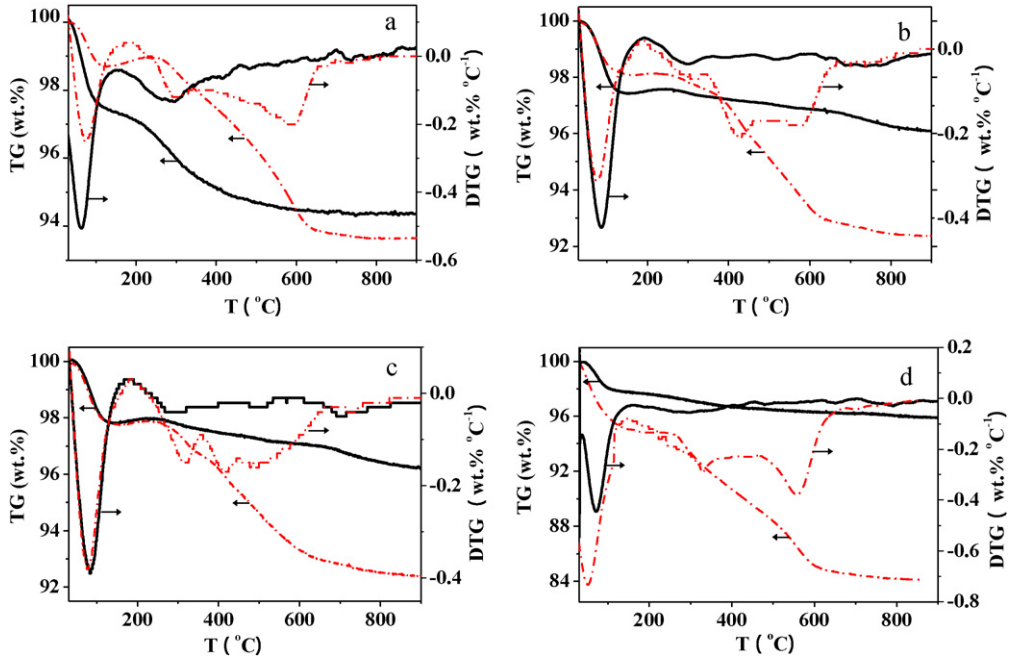

Fig. 5. TG and DTG curves for the original (solid lines) and phenyl-grafted (dashed lines) SBA-15 (a), MCM-41 (b), MCM-48 (c) and KIT-6 (d), respectively.

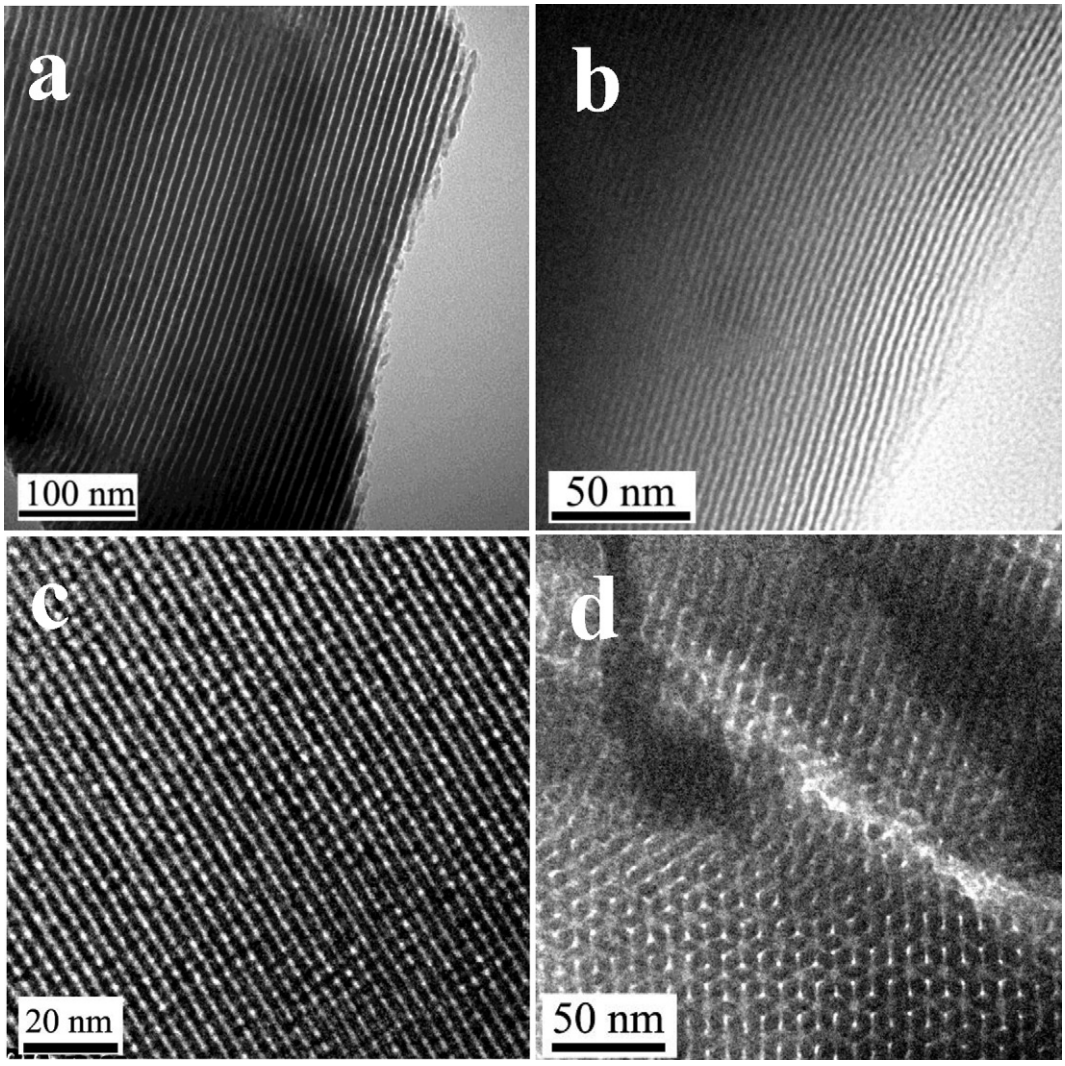

Fig. 6. Transmission electron microscopy (TEM) images of the phenyl-grafted SBA-15 (a), MCM-41 (b), MCM-48 (c) and KIT-6 (d).

more rapidly compared with all the other samples, implying less resistance in intraparticle mass transfer [10]. In contrast, the post-breakthrough sharpness of the increase in benzene concentration for the original and phenyl-grafted MCM-41 is the lowest, indicating relatively large mass transfer resistance. The single component dynamic adsorption results confirm that the pore size influences the mass transfer more significantly than the pore topology and the bicontinuous cubic pore (*Ia*3*d* mesostructure) is better than the parallel pore channel (2D hexagonal mesostructure).

The dynamic adsorption capacity of benzene on the adsorbent was calculated by integrating the area above the whole breakthrough curve. Table 2 summarized the dynamic adsorption capacities of benzene under dry (Q^{b}_{dry}) and humid environments ($Q^{b}_{13\%RH}$), as well as adsorption efficiency ($Q^{b}_{13\%RH}/Q^{b}_{dry}$) in the presence of water vapor. Under the dry condition, the adsorption capacities of phenyl-grafted samples are somewhat lower than the original samples, arising from the decrease in porosity owing to the partial pore blockage by the PTES species. Table 2 shows that the phenyl-grafted KIT-6 exhibits the highest adsorption capacity ($0.96\,mmol\,g^{-1}$) in the presence of water vapor. The adsorption efficiency of all the phenyl-grafted samples shows higher values than that of their original samples, suggesting the increase of the hydrophobicity and benzene adsorption capacity of the phenyl functionalized silicas. The adsorption efficiency of phenyl-grafted samples changes in the order of p-KIT-6 > p-SBA-15 > p-MCM-48 > p-MCM-41. Obviously, p-KIT-6 shows the highest efficiency towards benzene and its dynamic adsorption capacity under wet condition is 82% of its capacity under dry condition, which is likely attributed to the high degree of surface functionalization and the facilitated mass transfer in the relatively large and bicontinuous cubic mesopores. Therefore, the adsorption performance of aromatic compounds on the silica materials is strongly influenced by the surface chemistry and the pore structure. The excellent hydrophobicity of p-KIT-6 surface and bicontinuous cubic pore structure enable it to be a selective adsorbent for environmental applications, such as the removal of VOCs in the presence of water vapor.

3.3. Dynamic adsorption of bi-component

To further study the affinity between benzene molecules and phenyl groups on the surface of the adsorbents, simultaneous adsorption of benzene and cyclohexane on original and phenyl-grafted SBA-15, MCM-41, MCM-48 and KIT-6 was investigated. As shown in Fig. 8, the breakthrough time for benzene on all the samples are evidently longer than that for cyclohexane. Corre-

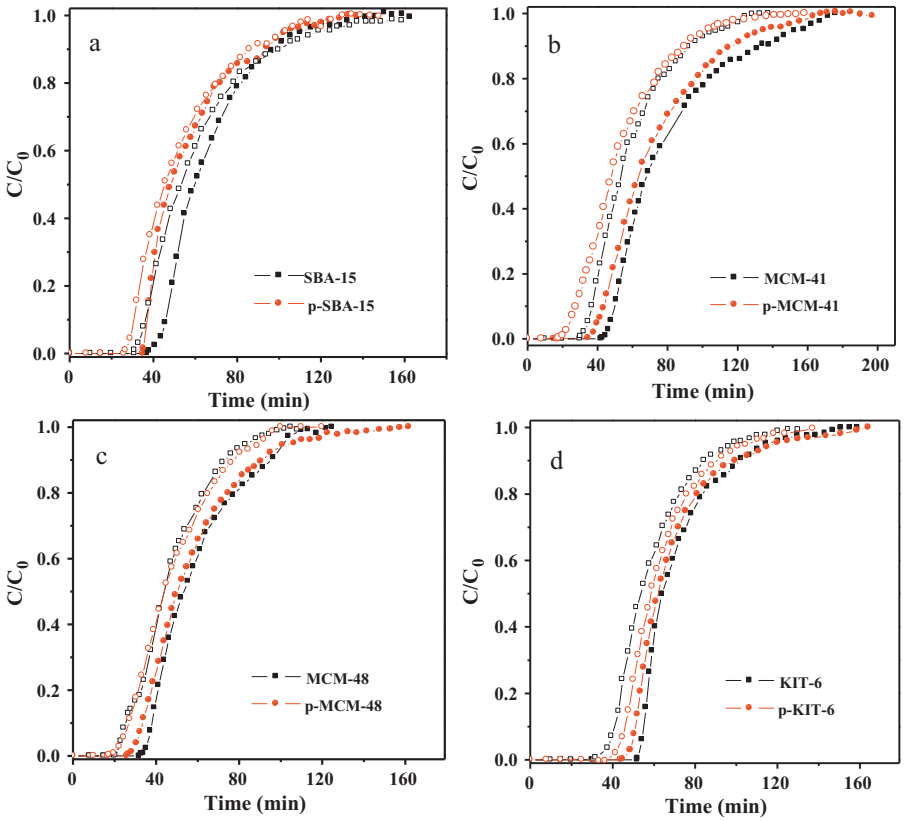

Fig. 7. The breakthrough curves of benzene on the original and phenyl-grafted SBA-15 (a), MCM-41 (b), MCM-48 (c) and KIT-6 (d), respectively. Curves with filled symbols represent results obtained under dry conditions and curves with empty symbols represent results obtained under wet conditions (13% RH).

spondingly, the dynamic adsorption capacity of benzene is larger than that of cyclohexane (Table 2). These observations can be explained by the different polarity degree of benzene and cyclohexane. Although cyclohexane possesses the same carbon atoms and a cyclic structure as benzene, the polarity of cyclohexane is less than that of benzene [29]. Benzene molecules are adsorbed preferentially on the surface of grafted samples with phenyl groups because they have the same π-electron structure and the π-electron effects make them strongly attract each other [39]. Nevertheless, a saturated cycloalkane (cyclohaxane) interacts with phenyl-grafted adsorbents weakly, leading to short breakthrough time and low dynamic adsorption capacity. From Table 2, phenyl-grafted SBA-15, MCM-41 and MCM-48 show systematically lower bi-component adsorption capacities as compared with their original samples, owing to the pore volume reduction. However, the bi-component adsorption capacity for phenyl-grafted KIT-6 is higher than that for its original sample. As shown in Fig. 8 and Table 2, p-KIT-6 exhibits the longest breakthrough time and the highest bi-component adsorption capacity, in accordance with the single component adsorption results. The best adsorption performance of p-KIT-6 can be attributed to the bicontinuous cubic pore structure and the highest degree of surface functionalization which leads to high affinity between aromatic compounds and the surface phenyl groups.

3.4. Static adsorption behaviors

The investigation of static adsorption and desorption behavior was conducted to further study the effects of surface chemistry on the adsorption properties. The adsorption and desorption isotherms of benzene on the original and phenyl-grafted SBA-15, MCM-41, MCM-48 and KIT-6 at 35 °C are displayed in Fig. 9. The shapes of adsorption and desorption isotherms for all the samples are similar to the nitrogen isotherms and can be classified into type IV. As shown in Fig. 9, the isotherms of benzene on the

Table 2
Dynamic adsorption capacities of the original and phenyl-grafted mesoporous materials.

Samples	Dynamic adsorption capacity Q (mmol g^{-1})					
	Single component			Bi-component		
	Benzene Q^b_{dry}	Benzene $Q^b_{13\%RH}$	$Q^b_{13\%RH}/Q^b_{dry}$ (%)	Cyclohexane Q^c	Benzene Q^b	Total VOCs Q^t
SBA-15	0.91	0.49	54	0.32	0.54	0.86
p-SBA-15	0.65	0.47	72	0.24	0.40	0.64
MCM-41	1.02	0.53	52	0.36	0.57	0.93
p-MCM-41	0.90	0.50	56	0.20	0.54	0.74
MCM-48	0.98	0.53	54	0.37	0.58	0.90
p-MCM-48	0.78	0.50	64	0.21	0.55	0.76
KIT-6	1.26	0.68	54	0.32	0.67	0.99
p-KIT-6	1.17	0.96	82	0.34	0.69	1.03

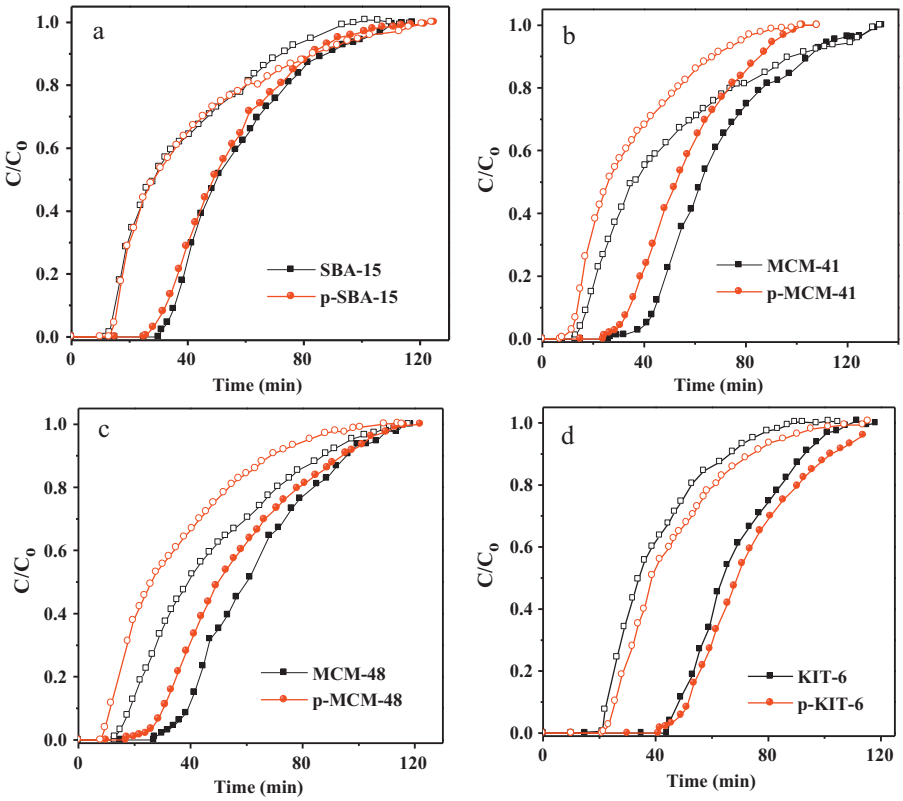

Fig. 8. The breakthrough curves of benzene (filled symbols) and cyclohexane (open symbols) on the original and phenyl-grafted SBA-15 (a), MCM-41 (b), MCM-48 (c) and KIT-6 (d), respectively.

phenyl-grafted samples remain the same as those on the original pure silicas, in spite of decrease in the adsorbed amount. Table 3 shows that the equilibrium adsorption capacities of benzene on phenyl-grafted samples are systematically lower than those on the original samples, corresponding to the reduction of the pore volume of functionalized samples. Particularly, KIT-6 presents the highest equilibrium adsorption capacity of 11.93 mmol g^{-1}, due to its high total pore volume (1.29 cm^3 g^{-1}). For p-KIT-6, the equilibrium adsorption capacity is 10.71 mmol g^{-1}, which is still higher compared with previous studies on mesoporous silica materials for benzene adsorption [10,21].

The Henry constants, which reflect adsorption affinity in the line region of the adsorption isotherm, can be estimated from the adsorption date at very low pressure ($P < 3$ mbar), where the interaction between adsorbed molecules may be neglected and only interactions between adsorbed molecules and the surface remain [40]. As can be seen in Table 3, the Henry constants for the adsorption of benzene on phenyl-grafted samples exhibit higher values compared with those on original pure silica samples, suggesting that the phenyl-grafted samples have stronger interaction with adsorbate. Furthermore, the following trend in Henry constant was observed for phenyl-grafted silicas: p-KIT-6 > p-SBA-15 > p-MCM-48 > p-MCM-41, in accordance with the degree of the surface functionalization. This observation further confirms that the large pore and cubic mesostructure are favorable to the diffusion of organosilane precursors, which leads to uniform distribution of organic functional groups on the surface of mesopores and the high degree of functionalization. On the other hand, the small mesopores and 1D mesoporous channels tend to cause some hindrance for the diffusion of organosilane precursors, resulting in the low degree of functionalization.

3.5. *Effects of surface chemistry and pore structure on adsorption performances*

As mentioned above, the surface chemistry and the pore structure play important roles in VOCs adsorption. The surface chemistry of mesoporous silicas can be effectively modified to be more hydrophobic and more lipophilic by the surface functionalization with organic groups. There is a relationship between adsorption performance and surface chemistry of the adsorbents. The dynamic adsorption results demonstrate that the functionalized silicas exhibit higher adsorption efficiency of benzene in the presence of water and higher adsorption capacity of bi-component (benzene and cyclohexane) than the original pure silicas. The static adsorption results further confirm that the functionalized silica surface has higher affinity for VOCs as compared with the original silica surface. Particularly, single-and bi-component dynamic adsorption properties and Henry constants derived from adsorption isotherms provide evidence that the phenyl-grafted KIT-6

Table 3
Equilibrium adsorption capacities Q^e (mmol g^{-1}) and Henry constants (K, 10^{-5} mol g^{-1} Pa^{-1}) of benzene on the original and phenyl-grafted SBA-15, MCM-41, MCM-48 and KIT-6 at 35 °C.

Samples	SBA-15	p-SBA-15	MCM-41	p-MCM-41	MCM-48	p-MCM-48	KIT-6	p-KIT-6
Q^e	10.64	9.98	7.28	6.13	9.39	7.97	11.93	10.71
K	0.09	0.20	0.07	0.16	0.06	0.18	0.14	0.28

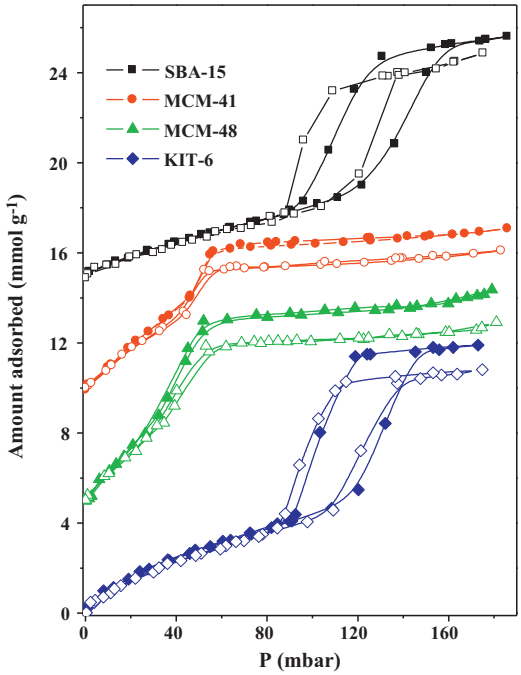

Fig. 9. Adsorption isotherms of benzene on the original (filled symbols) and phenyl-grafted (open symbols) SBA-15, MCM-41, MCM-48 and KIT-6 at 35 °C. The isotherms for the original and phenyl-grafted MCM-48, MCM-41 and SBA-15 are shifted by 5, 10 and 15 mmol g^{-1}, respectively.

has the highest adsorption capacity and affinity for benzene as compared with other phenyl-grafted samples. The best adsorption performance of p-KIT-6 can be explained by the highest degree of the surface functionalization. On the other hand, the relatively poor adsorption performance of p-MCM-41 probably attribute to the low degree of surface functionalization and partial pore blockage. The large mesopores and bicontinuous cubic mesostructure of KIT-6 can enhance the diffusion of PTES through the pores, leading to the uniform distribution of grafted phenyl groups and high degree of functionalization, as schematically shown in Fig. 1 where the surface group density for p-KIT-6 is higher than the others. However, the relatively small pore size and 2D hexagonal mesostructure of MCM-41 tend to cause some hindrance for PTES molecules to further diffuse inside the pores, which result in the phenyl groups anchoring near the entrance of the pores, in accordance with a previous report by Kailasam et al. [41]. In addition, the pore structure of mesoporous materials is another important factor influencing the adsorption performance. The dynamic adsorption results suggest that the highly interwoven and branched bi-continuous pore topology, as well as relatively large diameter, could provide more favorable mass transfer kinetics during the adsorption process. The unique advantages of pore structure, such as relatively large mesopore diameter and bicontinuous cubic mesostructure, make p-KIT-6 superior in adsorption performance and potentially useful for application as adsorbents for VOCs removal.

4. Conclusions

Phenyl functionalized ordered mesoporous silicas with different pore sizes and mesostructures were prepared by a post-synthesis grafting approach. Furthermore, the adsorption performances of VOCs on the original and functionalized mesoprous silicas were investigated. It was found that the phenyl groups are covalently anchored onto the surface of the mesoporous silicas while retaining their ordered mesostructures, and p-KIT-6 exhibits the highest degree of the surface functionalization. Adsorption results indicate that the adsorption efficiency of benzene on the functionalized samples in the presence of water is significantly improved and the phenyl functionalization can significantly enhance the surface hydrophobicity of the silica. Furthermore, the affinity between aromatic compounds and the surface phenyl groups leads to a high adsorption capacity of benzene. The large pore diameter and cubic pore structure are favorable to the surface functionalization and the good adsorption performance. In particular, p-KIT-6 offers the best performance in the dynamic adsorption which is likely attributed to its relatively large mesopores and bi-continuous cubic pore structure. The large pore and cubic mesostructure are favorable to the diffusion of organosilane precursors, leading to uniformly distributed organic functional groups on mesopore surface. Large pore size is also beneficial to the diffusion of adsorbate molecules, which can mitigate the diffusion restrictions. However, the functionalized MCM-41 exhibits the lowest adsorption efficiency than the other functionalized materials owing to the restricted size of the mesopores and 1D mesoporous channels. With excellent adsorption performance, the phenyl-grafted KIT-6 as a potential adsorbent would have a promising future in the field of VOCs removal, especially in the presence of water.

Acknowledgments

This study is financially supported by National Natural Science Fundation of China (20725723, 20807050), National Basic Research Program of China (2010CB732300), the National High Technology Research and Development Program of China (2006AA06A310) and the Australian Research Council (ARC) through Discovery Project program (DP0987969, DP1095861).

References

[1] M.E. Ramos, P.R. Bonelli, A.L. Cukierman, M.M.L. Ribeiro Carrott, P.J.M. Carrott, Adsorption of volatile organic compounds onto activated carbon cloths derived from a novel regenerated cellulosic precursor, J. Hazard. Mater. 177 (2010) 175–182.
[2] T. Yamamoto, S. Kataoka, T. Ohmori, Characterization of carbon cryogel microspheres as adsorbents for VOC, J. Hazard. Mater. 177 (2010) 331–335.
[3] R. Serna-Guerrero, A. Sayari, Applications of pore-expanded mesoporous silica. 7. Adsorption of volatile organic compounds, Environ. Sci. Technol. 41 (2007) 4761–4766.
[4] X.S. Zhao, Q. Ma, G.Q. Lu, VOC removal: comparison of MCM-41 with hydrophobic zeolites and activated carbon, Energy Fuels 12 (1998) 1051–1054.
[5] J.W. Lee, W.G. Shim, H. Moon, Adsorption equilibrium and kinetics for capillary condensation of trichloroethylene on MCM-41 and MCM-48, Micropor. Mesopor. Mater. 73 (2004) 109–119.
[6] W. Makowski, P. Kustrowski, Probing pore structure of microporous and mesoporous molecular sieves by quasi-equilibrated temperature programmed desorption and adsorption of n-nonane, Micropor. Mesopor. Mater. 102 (2007) 283–289.
[7] W. Rudzinski, J. Narkiewicz-Michalek, P. Szabelski, A.S.T. Chiang, Adsorption of aromatics in zeolites ZSM-5: a thermodynamic-calorimetric study based on the model of adsorption on heterogeneous adsorption sites, Langmuir 13 (1997) 1095–1103.
[8] S. Brosillon, M.H. Manero, J.N. Foussard, Mass transfer in VOC adsorption on zeolite: experimental and theoretical breakthrough curves, Environ. Sci. Technol. 35 (2001) 3571–3575.
[9] C.H. Christensen, K. Johannsen, I. Schmidt, Catalytic benzene alkylation over mesoporous zeolite single crystals: improving activity and selectivity with a new family of porous materials, J. Am. Chem. Soc. 125 (2003) 13370–13371.
[10] K. Kosuge, S. Kubo, N. Kikukawa, M. Takemori, Effect of pore structure in mesoporous silicas on VOC dynamic adsorption/desorption performance, Langmuir 23 (2007) 3095–3102.
[11] S.Z. Qiao, S.K. Bhatia, D. Nicholson, Study of hexane adsorption in nanoporous MCM-41 silica, Langmuir 20 (2004) 389–395.
[12] M. Hartmann, C. Bischof, Mechanical stability of mesoporous molecular sieve MCM-48 studied by adsorption of benzene, n-heptane and cyclohexane, J. Phys. Chem. B 103 (1999) 6230–6235.
[13] A. Stein, B.J. Melde, R.C. Schroden, Hybrid inorganic-organic mesoporous silicates-nanoscopic reactors coming of age, Adv. Mater. 12 (2000) 1403–1419.
[14] R. Ryoo, C.H. Ko, M. Kruk, V. Antochshuk, M. Jaroniec, Block-copolymer-templated ordered mesoporous silica: array of uniform mesopores or mesopore–micropore network, J. Phys. Chem. B 104 (2000) 11465–11471.
[15] K.P. Gierszal, T.W. Kim, R. Ryoo, M. Jaroniec, Adsorption and structural properties of ordered mesoporous carbons synthesized by using various carbon

precursors and ordered siliceous P6mm and Ia3d mesostructures as templates, J. Phys. Chem. B 109 (2005) 23263–23268.
[16] H. Vinh-Thang, Q. Huang, M. Eic, D. Trong-On, S. Kaliaguine, Adsorption of C_7 hydrocarbons on biporous SBA-15 mesoporous silica, Langmuir 21 (2005) 5094–5101.
[17] A. Matsumoto, K. Tsutsumi, K. Schumacher, K.K. Unger, Surface functionalization and stabilization of mesoporous silica spheres by silanization and their adsorption characteristics, Langmuir 18 (2002) 4014–4019.
[18] V. Kocherbitov, V. Alfredsson, Hydration of MCM-41 studied by sorption calorimetry, J. Phys. Chem. C 111 (2007) 12906–12913.
[19] C.M. Bambrough, R.C.T. Slade, R.T. Williams, Synthesis of a large pore phenyl-modified mesoporous silica and its characterization by nitrogen and benzene sorption, J. Mater. Chem. 8 (1998) 569–571.
[20] F. Hoffmann, M. Cornelius, J. Morell, M. Fröba, Silica-based mesoporous organic-inorganic hybrid materials, Angew. Chem. Int. Ed. 45 (2006) 3216–3251.
[21] X.S. Zhao, G.Q. Lu, Modification of MCM-41 by surface silylation with trimethylchlorosilane and adsorption study, J. Phys. Chem. B 102 (1998) 1556–1561.
[22] K. Inumaru, Y. Inoue, S. Kakii, T. Nakano, S. Yamanaka, Molecular selective adsorption of dilute alkylphenols and alkylanilines from water by alkyl-grafted MCM-41: tunability of the cooperative organic-norganic function in the nanostructure, Phys. Chem. Chem. Phys. 6 (2004) 3133–3139.
[23] T. Martin, A. Galarneau, F. Di Renzo, D. Brunel, F. Fajula, S. Heinisch, G. Cretier, J.L. Rocca, Great improvement of chromatographic performance using MCM-41 spheres as stationary phase in HPLC, Chem. Mater. 16 (2004) 1725–1731.
[24] H. Huang, C. Yang, H. Zhang, M. Liu, Preparation and characterization of octyl and octadecyl-modified mesoporous SBA-15 silica molecular sieves for adsorption of dimethyl phthalate and diethyl phthalate, Micropor. Mesopor. Mater. 111 (2008) 254–259.
[25] D. Zhao, J. Feng, Q. Huo, N. Melosh, G.H. Fredrickson, B.F. Chmelka, G.D. Stucky, Triblock copolymer syntheses of mesoporous silica with periodic 50 to 300 angstrom pores, Science 279 (1998) 548.
[26] H. Tian, J.J. Li, L. Zou, Z. Mu, Z.P. Hao, Removal of DDT from aqueous solutions using mesoporous silica materials, J. Chem. Technol. Biot. 84 (2009) 490–496.
[27] S.G. Wang, D. Wu, Y.H. Sun, B. Zhong, F. Deng, Y. Yue, Q. Luo, Synthesis of MCM-48 under high pressure, Acta Phys.: Chim. Sin. 17 (2001) 659–661.
[28] F. Kleitz, S.H. Choi, R. Ryoo, Cubic Ia3d large mesoporous silica: synthesis and replication to platinum nanowires, carbon nanorods and carbon nanotubes, Chem. Commun. 2003 (2003) 2136–2137.
[29] Q. Hu, J.J. Li, Z.P. Hao, L.D. Li, S.Z. Qiao, Dynamic adsorption of volatile organic compounds on organofunctionalized SBA-15 materials, Chem. Eng. J. 149 (2009) 281–288.
[30] A.J. Fletcher, E.J. Cussen, D. Bradshaw, M.J. Rosseinsky, K.M. Thomas, Adsorption of gases and vapors on nanoporous Ni_2 (4,4-bipyridine)$_3$(NO_3)$_4$ metal–organic framework materials templated with methanol and ethanol: structural effects in adsorption kinetics, J. Am. Chem. Soc. 126 (2004) 9750–9759.
[31] D. Zhao, J. Sun, Q. Li, G.D. Stuckys, Morphological control of highly ordered mesoporous silica SBA-15, Chem. Mater. 12 (2000) 275–279.
[32] A.S. Myong, H. Lim, Comparative studies of grafting and direct syntheses of inorganic–organic hybrid mesoporous materials, Chem. Mater. 11 (1999) 3285–3295.
[33] S. Han, J. Xu, W. Hou, X. Yu, Y. Wangs, Synthesis of high-quality MCM-48 mesoporous silica using gemini surfactant dimethylene-1,2-bis (dodecyldimethylammonium bromide), J. Phys. Chem. B 108 (2004) 15043–15048.
[34] Y. Zhai, B. Tu, D. Zhao, Organosilane-assisted synthesis of ordered mesoporous poly (furfuryl alcohol) composites, J. Mater. Chem. 19 (2009) 131–140.
[35] J.A. Bae, K.C. Song, J.K. Jeon, Y.S. Ko, Y.K. Park, J.H. Yim, Effect of pore structure of amine-functionalized mesoporous silica-supported rhodium catalysts on 1-octene hydroformylation, Micropor. Mesopor. Mater. 123 (2009) 289–297.
[36] B. Lei, B. Li, H. Zhang, L. Zhang, W. Li, Synthesis, characterization, and oxygen sensing properties of functionalized mesoporous SBA-15 and MCM-41 with a covalently linked ruthenium (II) complex, J. Phys. Chem. C 111 (2007) 11291–11301.
[37] C. Li, J. Liu, X. Shi, J. Yang, Q. Yang, Periodic mesoporous organosilicas with 1,4-diethylenebenzene in the mesoporous wall: synthesis, characterization, and bioadsorption properties, J. Phys. Chem. C 111 (2007) 10948–10954.
[38] X. Wang, S. Cheng, J.C.C. Chan, J.C.H. Chao, Template-free synthesis of mesoporous phenylsulfonic acid functionalized silica, Micropor. Mesopor. Mater. 96 (2006) 321–330.
[39] V.R. Choudhary, K. Mantri, Adsorption of aromatic hydrocarbons on highly siliceous MCM-41, Langmuir 16 (2000) 7031–7037.
[40] X. Lin, A.J. Blake, C. Wilson, X.Z. Sun, N.R. Champness, M.W. George, P. Hubberstey, R. Mokaya, M.J. Schroder, A porous framework polymer based on a zinc(II)4,4-bipyridine-2,6,2, 6-tetracarboxylate: synthesis, structure, and zeolite-like behaviors, J. Am. Chem. Soc. 128 (2006) 10745–10753.
[41] K. Kailasam, K. Müler, Physico-chemical characterization of MCM-41 silica spheres made by the pseudomorphic route and grafted with octadecyl chains, J. Chromatogr. A 1191 (2008) 125–135.